

Document downloaded from:

<http://hdl.handle.net/10251/64798>

This paper must be cited as:

Giménez Morales, C.; De La Torre, C.; Gorbe, M.; Aznar, E.; Sancenón Galarza, F.; Murguía, JR.; Martínez-Máñez, R.... (2015). Gated mesoporous silica nanoparticles for the controlled delivery of drugs in cancer cells. *Langmuir*. 31(12):3753-3762.
doi:10.1021/acs.langmuir.5b00139.



The final publication is available at

<http://dx.doi.org/10.1021/acs.langmuir.5b00139>

Copyright American Chemical Society

Additional Information

Gated mesoporous silica nanoparticles for the controlled delivery of drugs in cancer cells

Cristina Giménez,^{†,§} Cristina de la Torre,^{†,§} Mónica Gorbe,^{†,§} Elena Aznar,^{†,§} Félix Sancenón,^{†,§‡} Jose R. Murguía,^{†,§,B} Ramón Martínez-Mañez,^{*†,§,‡} M. Dolores Marcos,^{†,§,‡} and Pedro Amorós^ϕ*

[†] Centro de Reconocimiento Molecular y Desarrollo Tecnológico (IDM) , [‡] Departamento de Química and ^B Departamento de Biotecnología, Universitat Politècnica de València, Valencia, 46022, Spain

[§]CIBER de Bioingeniería, Biomateriales y Nanomedicina (CIBER-BBN), Valencia, Spain

^ϕInstitut de Ciència dels Materials (ICMUV), Universitat de València, P.O. Box 2085, E-46071, Valencia, Spain

ABSTRACT: In recent years, mesoporous silica nanoparticles (MSN) have been used as effective supports for the development of controlled release nanodevices able to act as a multifunctional delivery platform for the encapsulation of therapeutic agents, enhancing their bioavailability and overcoming common issues such as poor water solubility and poor stability of some drugs. In particular, redox-responsive delivery systems have attracted the attention of scientists because of the intracellular reductive environment related with a high concentration of glutathione (GSH). In this context we describe herein the development of a GSH-responsive delivery system based in PEG-capped MSN able to deliver safranin O and doxorubicin in a controlled manner. The results showed that the PEG-capped systems designed in this work can

be maintained closed at low GSH concentrations yet the cargo is delivered when the concentration of GSH increased. Moreover, the efficacy of the PEG-capped system in deliver the cytotoxic agent doxorubicin in cells was also demonstrated.

INTRODUCTION

Since its beginning, nanotechnology has revolutionized each field in which it has been exploited. In the area of medicine, it offers a broad variety of tools able to transform and improve conventional therapeutic and diagnostic strategies. In particular, one of the fields within medicine in which nanotechnology has a great potential is the development of new smart drug delivery systems able to release therapeutic agents in a controlled and selective manner. With this, researchers aim to prepare effective supports for the development of controlled release nanodevices able to act as a multifunctional delivery platform for the encapsulation of therapeutic agents, enhancing their bioavailability and overcoming common issues such as poor water solubility, poor stability of some drugs and undesired side effects. This goal is especially appealing in the delivery of cytotoxic drugs for cancer treatment. Based in these concepts, a number of nanodevices for encapsulation, transport and release of antineoplastic agents have been described based on different platforms such as liposomes, polymeric nanoparticles, lipid-polymer hybrid nanoparticles, dendrimers and inorganic nanoparticles.¹⁻¹⁰ In most cases it was observed that these drug nanocarriers tend to accumulate at solid tumour sites due to their comparatively leaky vasculature and poor lymphatic drainage. These properties make the tumour vasculature hyperpermeable for high molecular weight (≤ 40 kDa) long-circulating macromolecules and nanoparticles. This effect, known as the enhanced permeation and retention

effect (EPR), results in a passive targeting that allow achieving higher intratumoral drug concentration and decreasing the toxicity in normal tissues.¹¹⁻¹⁴

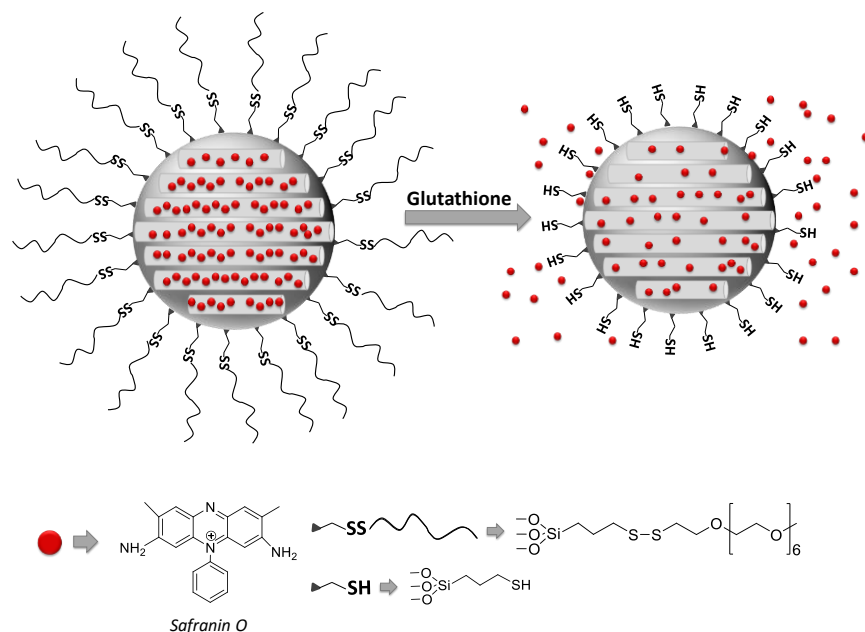
In recent years, mesoporous silica nanoparticles (MSN) have been used as effective support for the development of controlled release nanodevices due to their unique characteristics, such as high homogeneous porosity, inertness, robustness, thermal stability and high loading capacity. Owing to their properties, these supports are able to act as multifunctional delivery platforms for the encapsulation of therapeutic agents.¹⁵⁻¹⁷ Moreover, MSN could be decorated with switchable “gate-like” ensembles on the external surface, capable of being “opened” or “closed” upon the application of certain external stimuli.¹⁸ These concepts have allowed the design of nanodevices for on-command delivery that can be triggered by target chemical (such as redox molecules,¹⁹⁻²¹ selected anions²²⁻²⁴ and pH changes²⁵⁻²⁸), physical (such as light,²⁹⁻³¹ temperature³²⁻³⁵ or magnetic fields³⁶⁻³⁸) and biochemical (such as enzymes,³⁹⁻⁴³ antibodies,⁴⁴ or DNA^{45,46}) stimuli.

In this context redox-responsive delivery systems are particularly appealing because intracellular release of therapeutic agents can be achieved by the reductive environment of the cytosol tied with a high concentration of glutathione (GSH). In fact, since Lin and coworkers reported the first redox-responsive gated material in which cadmium nanoparticles blocked the pore entrances of a silica mesoporous support and the release of the entrapped fluorescein was triggered by the rupture of a disulphide bond,⁴⁷ several capped systems driven by GSH and other reducing agents have been described.⁴⁸⁻⁵⁴ GSH is a thiol-containing tripeptide capable of reducing disulfide bonds, and its intracellular concentration (10mM) is significantly higher than its concentration in blood plasma (2μM).⁵⁵ These differences in GSH concentration inside and outside the cell allows the design of GSH-driven nanovalves for drug transport that remain

closed in extracellular environments whereas they open and deliver their cargo in intracellular medium. Moreover, the GSH levels in some cancer tissues have been found many-fold higher than those in normal tissues.^{56, 57}

In the same context, the preparation of controlled release nanodevices able to remain stable and bioavailable for long time in the human body environment is a pursued goal. In this field, polyethylene glycol (PEG) has been widely used. This molecule is a highly hydrophilic polymer currently and thoroughly used in drug delivery formulations. It has been demonstrated that PEGylation of nanoparticles increases its solubility in buffer and serum due to the hydrophilic ethylene glycol moieties. Moreover, the presence of PEG groups on the surface of nanoparticles reduces the nonspecific binding of nanoparticles to blood proteins and macrophages, resulting in the so-called “stealth” behaviour. As a result, it has been described that the blood circulation half-lives of PEG-containing nanocarriers are prolonged and the passive targeting to cancer cells tied with EPR effect could be enhanced.

Based in these concepts, our aim was to design a GSH-responsive gated material, based on MSN, as a simple to prepare and stable delivery systems of cytotoxic agents. In particular, we report herein the preparation of a hybrid material consisting of MSN loaded with a cargo (a dye or drug) and functionalized with PEG chains in the pore outlets using a disulfide linkage. The proposed paradigm is depicted in Scheme 1. It was expected that the size of PEG chains would be enough to block the pores and to inhibit cargo release. Moreover, as illustrated in Scheme 1, the presence of the intracellular reducing agent GSH is expected induce the uncapping of the pores and the delivery of the entrapped guest.



Scheme 1. Schematic representation of the gated material **S1** capped with PEG chains via disulfide linkage.

EXPERIMENTAL SECTION

Synthesis of mesoporous MCM-41 nanoparticles

Mesoporous MCM-41 nanoparticles were synthesised by the following procedure: n-cetyltrimethylammonium bromide (CTAB, 1.00 g, 2.74 mmol) was first dissolved in deionized water (480 mL). Then, NaOH (3.5 mL, 2.00 mol L⁻¹) in deionized water was added to the CTAB solution, followed by adjusting the solution temperature to 80 °C. TEOS (5.00 mL, 2.57 x 10⁻² mol) was then added dropwise to the surfactant solution. The mixture was stirred for 2 h to give a white precipitate. Finally, the solid product was centrifuged, washed with deionized water and ethanol, and dried at 60 °C (MSN as-synthesized). To prepare the final porous nanoparticles

(calcined MSN), the as-synthesized solid was calcined at 550 °C using an oxidant atmosphere for 5 h in order to remove the template phase.

Synthesis of S1 and S2

For the preparation of solids **S1** and **S2**, 500 mg of calcined MSN and safranin O dye (140.34 mg, 0.40 mmol) were suspended in distilled water (17 mL) in a round-bottomed flask. The mixture was sonicated in an ultrasonic bath for 10 minutes and stirred for 24 h at room temperature, filtered off and dried under vacuum. Afterward, this loaded solid (250 mg) was re-suspended in acetonitrile (8.5 mL) in the presence of an excess of safranin O and (3-mercaptopropyl) trimethoxysilane (464.38 µL, 2.5 mmol) was added. The suspension was stirred for 5.5 h at room temperature and then, 2,2'-dipyridyl disulfide (550.77 mg, 2.5 mmol) was added to the reaction mixture. After stirring for 12 h at room temperature, the resulting solid was filtered off and dried under vacuum. Finally, a mixture of this prepared solid (50 mg) and O-(2-mercaptoethyl)-O'-methyl-hexa(ethylene glycol) (1.4 mmol) for **S1**, or poly(ethylene glycol)methyl ether thiol (0.15 mmol) for **S2** were suspended in acetonitrile (3.33 mL) in the presence of an excess of safranin O. The mixture was stirred for 12 h and the final materials **S1** and **S2** were isolated by centrifugation, washed with abundant water and dried at 40°C for 12 h. The prepared solids were easily redispersed by 1 min of mild sonication in an ultrasonic bath.

Synthesis of S3

Solid **S3** was prepared following the same procedure described for **S1** but, in this case, MSN was loaded with doxorubicin drug instead of safranin O. Then, 50 mg of calcined MSN and doxorubicin (10 mg, 0.017 mmol) were suspended in distilled water (0.8 mL) in a round-bottomed flask. The mixture was stirred for 24 h at room temperature, isolated by centrifugation

and dried under vacuum. Afterward, this loaded solid was re-suspended in acetonitrile (1.7 mL) and (3-mercaptopropyl) trimethoxysilane (92.87 μL , 0.5 mmol) was added. The suspension was stirred for 5.5 h at room temperature and then, 2,2'-dipyridyl disulfide (136.0 mg, 0.5 mmol) was added to the reaction mixture. After stirring for 12 h at room temperature, the resulting solid was isolated by centrifugation and dried under vacuum. Finally, a mixture of this prepared solid (28 mg) and O-(2-mercaptoethyl)-O'-methyl-hexa(ethylene glycol) (mPEG thiol) (113.12 μL , 0.08 mmol) were suspended in acetonitrile (1.885 mL) and the mixture was stirred for 12 h at room temperature. The final capped solid **S3** was isolated by centrifugation, washed with abundant water and dried under vacuum for 24 h. The prepared solid was easily redispersed by 1 min of mild sonication in an ultrasonic bath.

Dye release studies

Delivery experiments were carried out using the capped materials **S1**, **S2** and **S3**, in the absence or presence of glutathione (GSH) as reducing agent. In a typical experiment, 0.5 mg of each material were suspended in 1.125 mL of distilled water at pH 7.5. After sonication, 125 μL of the corresponding GSH stock solution were added. The suspension was then stirred and, at a certain time, an aliquot was separated and centrifuged. Dye and drug delivery was monitored through the emission band of safranin O or doxorubicin centred at 585 nm ($\lambda_{\text{exc}} = 520$ nm) and 557 nm ($\lambda_{\text{exc}} = 495$ nm) respectively.

Cell culture conditions

The HeLa human cervix adenocarcinoma cells were purchased from the German Resource Centre for Biological Materials (DSMZ). HeLa cells were routinely grown in DEM supplemented with 10% FBS, at 37 °C in an atmosphere of 5% CO₂ and underwent passage twice a week.

WST-1 cell viability assay

Cells were cultured in sterile 24-well microtiter plates at a seeding density of 25×10^3 cells/well for HeLa and were allowed to settle for 24h. **S1** or **S3** was added to the cells at a final concentrations of 20, 50, 150 and 200 μM . After 22 h, WST-1 (30 μL of a 50 mg/ml solution) was added to each well. Cells were further incubated for 2 h (a total of 24 h of incubation was therefore studied), and then shaken thoroughly for 1 minute on a shaker. After that, absorbance was measured at 450 nm against a background control as blank using a microplate ELISA reader. The reference wavelength was 690 nm.

Live confocal microscopy S1 and S3 cellular internalisation assays

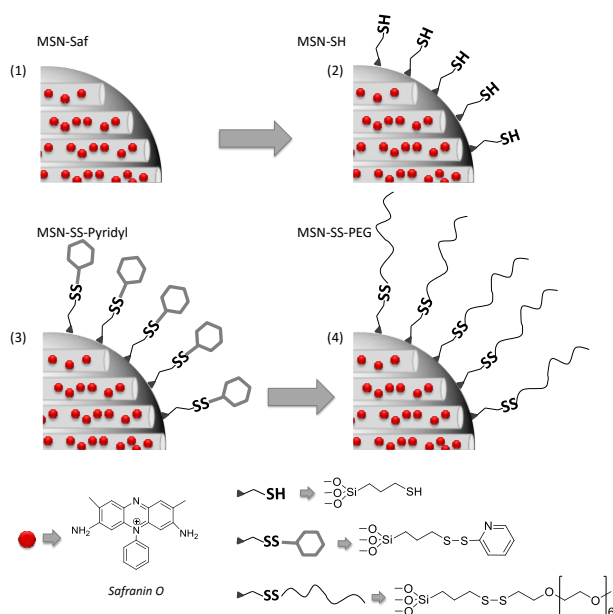
HeLa cells were seeded in 24 mm glass coverslips in 6-well microliter plates at a seeding density of 1.5×10^5 cells/well. After 24 hours, cells were treated with 75 $\mu\text{g/ml}$ of **S1** or **S3**. After 20 minutes, the medium was removed to eliminate compounds and washed with PBS. Then, cells were incubated during 20 hours at 37 °C, and were visualized under a confocal microscope. Confocal microscopy studies were performed with a Leica TCS SP2 AOBS (Leica Microsystems Heidelberg GmbH, Mannheim, Germany) inverted laser scanning confocal microscope using oil objectives: 63X Plan-Apochromat-Lambda Blue 1.4 N.A. Two-dimensional pseudo colour images (255 colour levels) were gathered with a size of 1024x1024 pixels and Airy 1 pinhole diameter. All confocal images were acquired using the same settings. Identical experiments were done three times to obtain reproducible results.

RESULTS AND DISCUSSION

Design and synthesis of gated MSN

In this study, we selected spherical nanometric MSN from the MCM-41 family as support. This is a suitable inorganic matrix that displays several appropriate characteristics, such as homogeneous porosity, high inertness and ease of functionalization. Moreover, typical MCM-41 materials contain mesopores in the 2–3 nm range, which allows the storage of a wide variety of guests. In relation to the capping ensemble, as stated above, we aimed to develop a gate-like platform that could be triggered by the GSH present in cells. As capping molecules we selected two different sized polyethylene glycol chains of molecular weights of 350 and 800, containing a terminal thiol group. Moreover different solids loaded with safranin O (**S1** and **S2**) or with doxorubicin (**S3**) were prepared. MSN were synthesised by using tetraethyl orthosilicate (TEOS), which acts as an inorganic precursor, and hexadecyltrimethylammonium bromide (CTAB) as a structure-directing agent. The subsequent removal of the surfactant by calcination in air at high temperature resulted in the starting mesoporous inorganic nanoparticles. To prepare the capped material containing the dye Safranin O in the pore voids and the 350 Mn PEG in the pore outlets (**S1**), we followed a four-step synthetic procedure (see Scheme 2). As a first step, calcined MSN were added to a water solution containing a high safranin O concentration and were stirred for 24 h to achieve an efficient loading of pores. The loaded solid was treated with 3-mercaptopropyltrimethoxysilane and then with 2,2'-dipyridyl disulfide to obtain 2-pyridinyldisulfanylpropyl-functionalized MSN. Finally, grafting of polyethylene glycol chains onto the external surface was achieved through the formation of a disulfide linkage by reaction with O-(2-mercaptoethyl)-O-methyl-hexa(ethyleneglycol). The nanoparticles were washed with abundant water and dried under vacuum to obtain the final solid **S1**. The hybrid material **S2** was

synthesized following the same procedure as **S1**, but in this case, PEG of a molecular weight of 800 was used. Finally, PEG-capped doxorubicin-containing hybrid material **S3** was prepared following the same procedure as **S1**, but using the drug doxorubicin as cargo.



Scheme 2. Synthetic route for preparing the final solid **S1**.

Characterization of the hybrid materials

The prepared solids were characterized using standard techniques. Powder X-ray diffraction (PXRD) patterns of the as-synthesized MSN, calcined MSN, and the final materials **S1**, **S2** and **S3** are shown in Figure 1. As it can be appreciated, the PXRD of synthesized MSN (Figure 1a) shows the four low-angle reflections attributed to the typical MCM-41 hexagonal array that can be indexed as (100), (110), (200), and (210) Bragg peaks. From these data, a d_{100} spacing of 42.25 Å can be calculated. In a further step, the PXRD of calcined MSN (Figure 1b) shows a significant displacement of the (100) peak, that can be attributed to an approximate cell contraction of 3.64 Å. This displacement and broadening of the (110) and (200) peaks found in

calcined MSN is related to further condensation of silanol groups during the calcination step. Finally, Figures 1c to 1e show the PXRD patterns for solid **S1**, **S2** and **S3** respectively. In these curves, the reflections (110) and (200) are practically lost, most likely due to a reduction in contrast as a consequence of the pore loading with the Safranin O dye (for **S1** and **S2**) or doxorubicin (for **S3**) and the functionalization with the corresponding polyethylene glycol chains. Nevertheless, the presence of the (100) peak in the PXRD pattern indicated that the process of pore loading and the additional functionalization with PEG did not modify the mesoporous structure of the MSN support in a large extent. The mesoporous structure of the prepared solids was also confirmed using transmission electron microscopy (TEM) analysis. As it can be observed in representative images of Figure 1, for solids **S1** and **S2**, MSN were obtained as spherical particles with a diameter of ca. 90 nm. Moreover, the typical MCM-41-like hexagonal arrangement of the mesopores can also be observed.

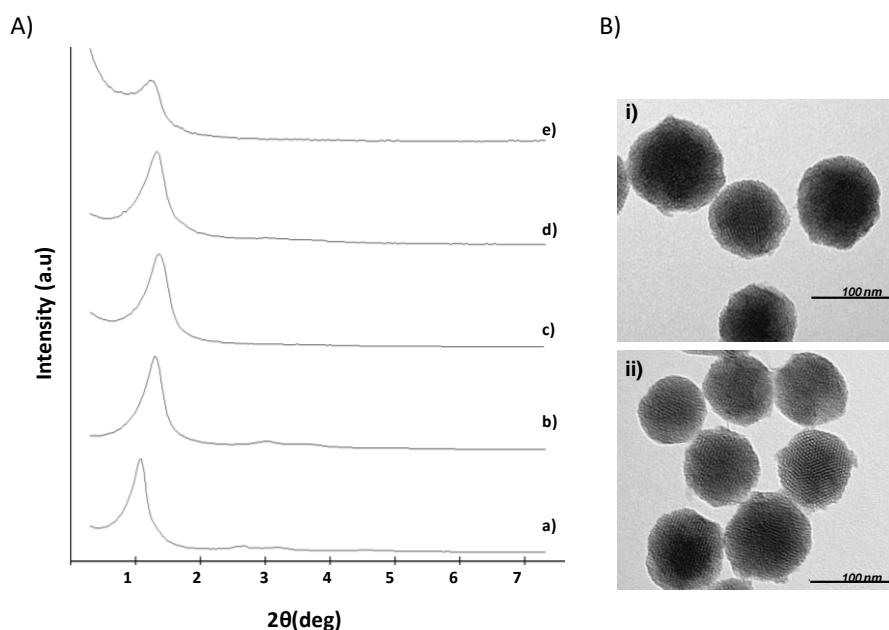


Figure 1. A) Powder X-ray pattern of a) MSN, b) calcined MSN, c) solid **S1** containing safranin O and functionalized with PEG (Mn 350), d) solid **S2** containing safranin O and functionalized with PEG (Mn 800) and e)

solid **S3** containing doxorubicin and functionalized with PEG. B) Transmission electron microscopy (TEM) images of i) solid **S1**, and ii) solid **S2** showing the typical porosity of the MCM-41 matrix.

In addition, N₂ adsorption–desorption isotherms of calcined MSN were registered. As it can be seen in Figure 2a, a typical curve for MCM-41-like mesoporous solids was obtained. In particular, a sharp adsorption step was recorded at intermediate P/P₀ values (0.25–0.4). This feature corresponds to a type IV isotherm, indicating the nitrogen condensation inside the mesopores by capillarity. Moreover, the free nitrogen release from the mesopores is confirmed by the absence of a hysteresis loop in this interval, suggesting the presence of uniform cylindrical mesopores. Using the adsorption branch of the porosimetry data, the Barrett–Joyner–Halenda (BJH)⁵⁸ model was applied and a narrow pore distribution centred at 2.76 nm was calculated. Furthermore, the application of the Brunauer, Emmett and Teller (BET) model resulted in a value of 1045.7 m²g⁻¹ for the total specific surface of calcined MSN. Taking into account the registered PXRD, porosimetry and TEM studies, an a₀ cell parameter of 4.45 nm and a wall thickness of 1.69 nm were calculated. These values are in agreement with typical MCM-41-type solids. In addition to the adsorption step associated to the micelle generated mesopores, a second feature can also be observed at a high relative pressure (P/P₀>0.85). This adsorption corresponds to the filling of the large voids among the particles and a main pore diameter of 49.63 nm can be calculated in this case by using the BJH model.

N₂ adsorption-desorption isotherms for the capped solids **S1**, **S2** and **S3** showed no remarkable steps at low-intermediate relative pressure values if compared to the calcined MSN. When BET and BJH models were applied lower N₂ adsorbed volume and surface areas were found (see Table SI-1, Supporting Information) for solids **S1**, **S2** and **S3** as expected when

compared with the starting MSN supports and due to the partial filling of the mesopores with the cargo.

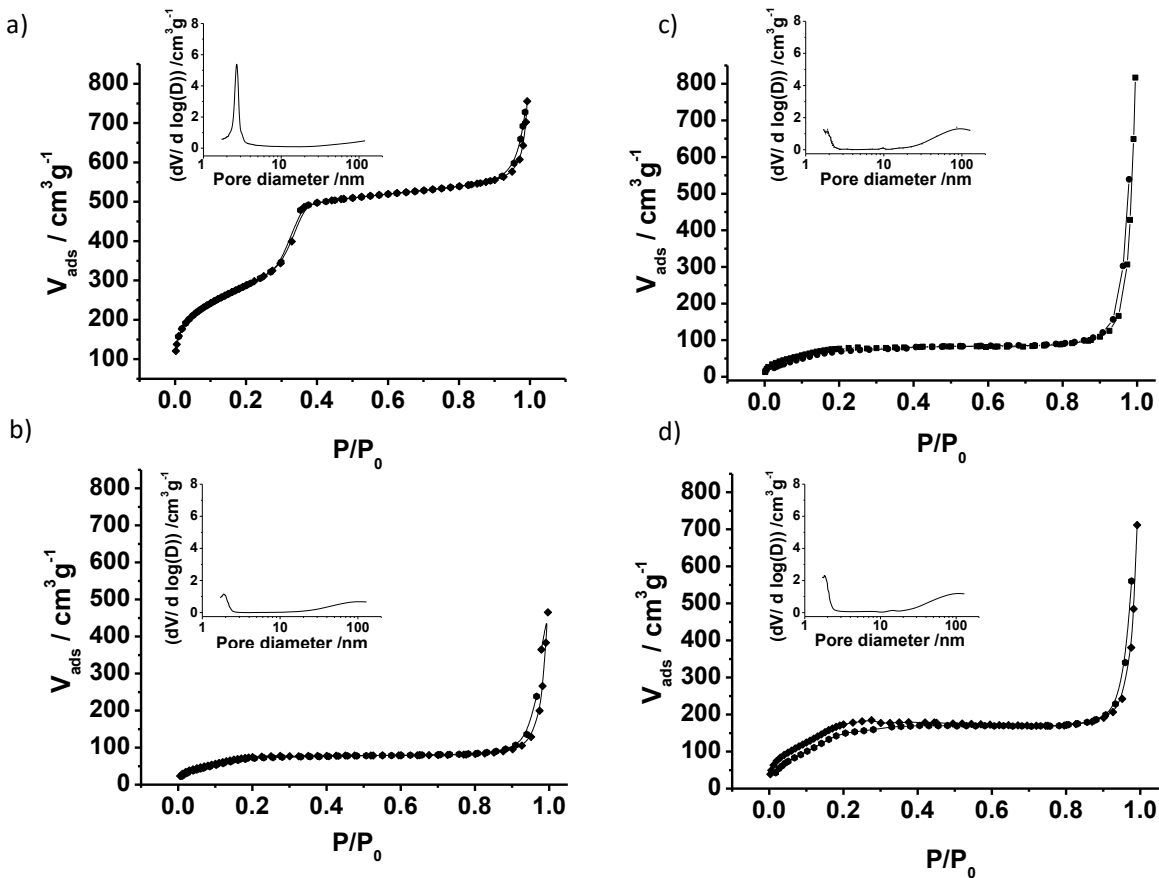


Figure 2. N₂ adsorption–desorption isotherms for a) MSN, b) S1, c) S2 and d) S3. Inset: Pore-size distribution for each corresponding solid.

Furthermore, the hydrodynamic diameter of calcined MSN, **S1** and **S2** was determined from Dynamic Light Scattering (DLS) studies (Figure SI-1, Supporting Information). The diameter for calcined MSN was of ca. 94 nm while that found for **S1** was higher (126 nm). An even larger diameter was registered for **S2** (178 nm). These results are in agreement with the functionalization of the MNS nanoparticles and with the larger size of the PEG derivative used to cap **S2** when compared with the PEG used to prepare **S1**.

Finally, the organic content in solids **S1**, **S2** and **S3** was determined by elemental analysis and thermogravimetric studies. Table SI-2 in Supporting Information summarizes all the obtained data. Specifically, a content of 0.11 and 0.21 mmol g⁻¹ SiO₂ of safranin O dye in solids **S1** and **S2** respectively and a content of 0.27 mmol g⁻¹ SiO₂ of doxorubicin in solid **S3** were obtained. All the obtained values are within the range usually observed in previously reported gated systems.

The Functional Redox-Responsive Controlled Release

As stated above, it was our aim the design of delivery systems triggered by a reductive environment in cells due to the presence of glutathione. In a first step release experiments in an aqueous solution were carried out with nanoparticles **S1** and **S2**. For example in a typical experiment **S1** material was suspended in water at pH 7.5 both, in the absence and presence of GSH (10mM). At certain fixed times, aliquots were separated, filtered and the delivery of safranin O dye from the pore voids was observed via monitoring of the fluorescence band of safranin O at 585 nm ($\lambda_{ex}=520$ nm) in the aqueous phase (see Figure 3). Solid **S1** displayed a poor release profile (curve a) in water, whereas it delivered the dye in the presence of GSH

(curve b). In particular **S1** nanoparticles were able to remain stable at least for 24 h in a non-reductive environment, whereas in the presence of 10mM GSH, a fast release of cargo was observed achieving 90% of the maximum release of the entrapped guest, corresponding to a 55% of the total loaded cargo, in less than 1 h. These results indicate that the anchored PEG chains form a dense barrier that inhibits cargo release effectively. In contrast, when GSH is present, the disulfide bond is cleaved allowing the release of the entrapped cargo.

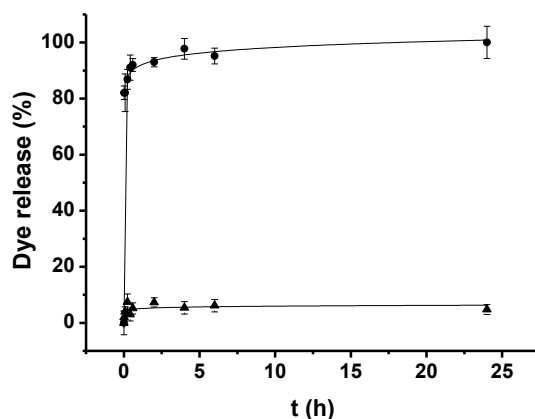


Figure 3. Kinetics of the release of safranin O from gated solid **S1** in water a) in the absence of GSH and b) in the presence of 10 mM GSH.

Once proved the suitable behaviour of the capped design, we studied the influence of GSH concentration in the release of safranin O from **S1**. The percentage of safranin O released after 24 h in the presence of different concentrations of GSH is shown in Figure 4. As expected the amount of released safranin O from **S1** was GSH-concentration dependent. Furthermore, stability of **S1** in other competitive media such as phosphate buffered saline (pH 7.4) and simulated body plasma (SBP) was explored. As it can be appreciated in Figure 4, in the absence of GSH the leakage of safranin O from **S1** pore voids was negligible. The results obtained indicated that **S1**

would remain tightly capped at typical GSH concentrations in plasma (ca. $2\mu\text{M}$), whereas is expected to display cargo delivery at intracellular GSH concentrations (ca. 10mM).

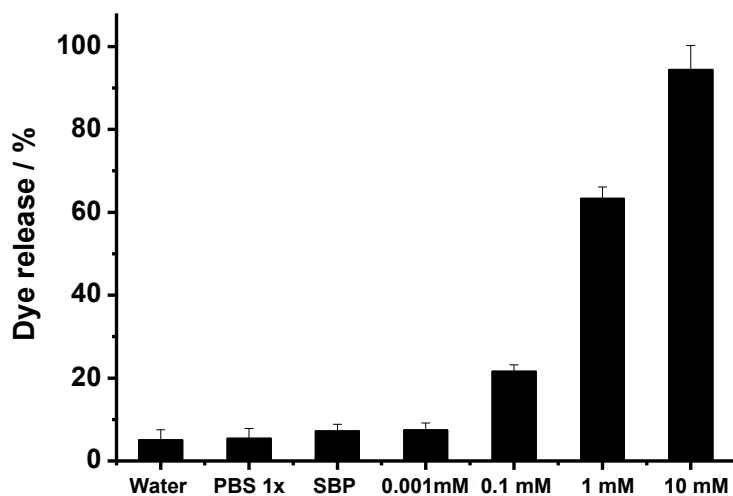


Figure 4. Relative fluorescence intensity of safranin O released from **S1** measured at 580 nm ($\lambda_{\text{ex}}=585$ nm) in water (pH 7.4), PBS 1x and SBP (pH 7.25), and in water (pH 7.4) as a function of GSH concentration.

Using a similar experimental procedure the release behaviour of **S2**, capped with a longer PEG (Mn 800) derivative, was also studied. The difference in emission of safranin O in the presence and absence of GSH is displayed in Figure 5. The release profile of **S2** was very similar to that observed for **S1**; i.e. a poor release in absence of glutathione (curve a) and a fast cargo delivery in the presence of 10mM GSH. The observed behaviour is consistent with the fact that the disulfide linker is positioned at the same relative distance of the surface as in solid **S1** and therefore both solids display a very similar delivery behaviour.

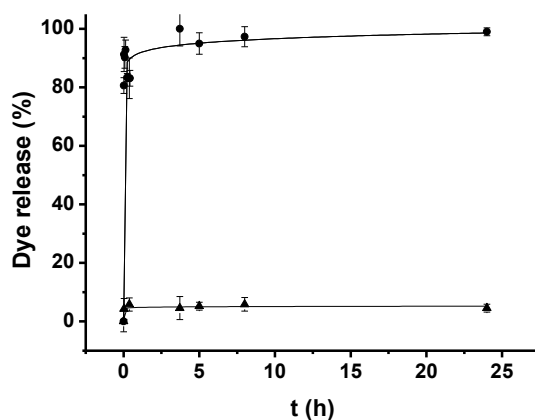


Figure 5. Kinetics of the release of safranin O dye from suspensions of gated solid **S2** in water a) in the absence of GSH and b) in the presence of GSH 10mM.

Using a similar experimental protocol, delivery from solid **S3**, containing the drug doxorubicin, was studied in water both in the absence and presence of GSH. In this case cargo delivery was monitored through the fluorescence band of doxorubicin at 557 nm ($\lambda_{exc} = 495$ nm). The obtained experimental results are shown in Figure 6. As above a flat baseline was found in the absence of glutathione, while a rapid cargo release was observed in the presence of GSH.

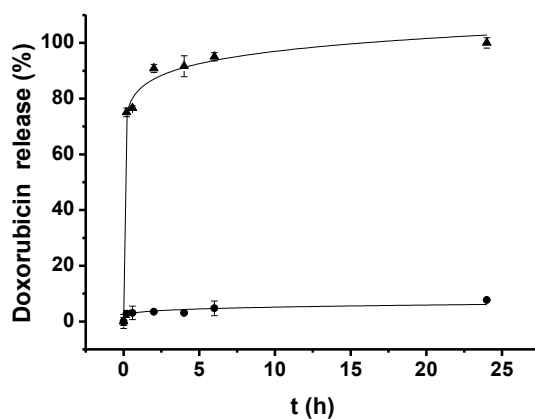


Figure 6. Kinetics of the release of doxorubicin from solid **S3** a) in the absence of GSH and b) in the presence of GSH 10mM.

Delivery in intracellular media

After the in vitro characterization the capped mesoporous **S1** and **S3** nanoparticles were used for further ex vivo assays. For these experiments, the tumour cell line HeLa was used. Cells were seeded in 6-well culture plates at a density of 150000 cells per well and allowed to adhere for 24 h. After that time, cells were incubated with solid **S1** at a final concentration of 75 $\mu\text{g}/\text{mL}$ for additional 24h. In these experiments, cells were also stained with the DNA-associated dye Hoechst 33342. The cellular uptake and intracellular release of **S1** was determined by confocal laser scanning microscopy (CLSM) by tracking safranin O associated fluorescence. As shown on Figures 7A and 7B, safranin O associated fluorescence (red) was clearly observed in the cellular cytosolic compartment indicating the internalization of nanoparticles, the rupture of the disulphide bond by the reductive environment, and the subsequent release of the entrapped dye.

Further studies with **S1** were performed to exclude any toxic effect. HeLa cells were treated with **S1** for 24 h at final concentrations of 20, 50, 150 and 200 $\mu\text{g}/\text{mL}$, respectively. After that time, a cell viability assay using WST-1 was performed. This yellow reagent (tetrazolium salt) can be reduced by mitochondrial enzymes to give a soluble orange product (formazan salt). This conversion only occurs in viable cells. Therefore, measuring the absorbance at 450 nm against a background control allows an accurate measurement of the number of metabolically active cells in the culture. As expected from previous reports^{35, 39, 42}, treatment of cells with **S1** nanoparticles showed non-toxicity effect in concentrations up to 200 $\mu\text{g}/\text{ml}$ after 24 hours (Figure 7C).

To further characterize cargo delivery from **S1** in cells the internalization of nanoparticles, we performed a time course experiment of dye release in HeLa cells. Accordingly 20 minutes after

incubation with **S1** material, cell culture medium was removed and cells were washed with PBS. Then, slides were mounted and visualized by confocal microscopy. Series of images of the same XY field were taken every two minutes. The obtained images revealed that the nanoparticles gradually internalized into cells, and produced a bright red fluorescence that increase in cells as a function of lapsed time (data not shown).

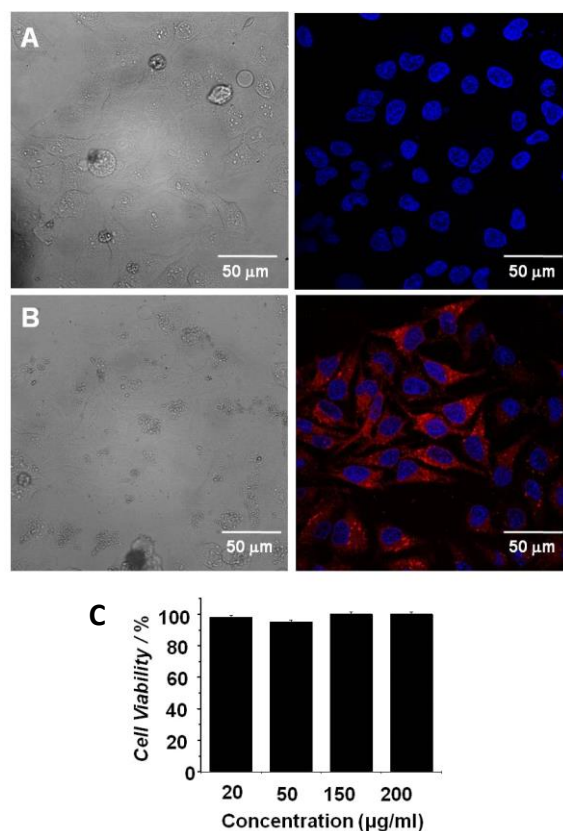


Figure 7. Cell viability and cellular internalization of **S1** gated-nanoparticles. a) Confocal microscopy images corresponding to untreated HeLa cells as a control of autofluorescence, and b) HeLa cells treated with solid **S1** at 75 µg/mL concentration. The cellular uptake of the nanoparticles was evidenced by safranin O associated fluorescence (red) in the presence of DNA marker Hoechst 33342 (blue). c) WST-1 cell viability assay. HeLa cells were incubated for 24 h with **S1** at the indicated concentrations. Cell viability was quantified by employing the WST-1 reagent. Three independent experiments each one done in duplicates were performed and the data are represented as (mean ± SE).

Once studied the intracellular uptake and performance of the gated material **S1**, HeLa cells were also used to demonstrate the possible cellular internalization of **S3** and its ability to release loaded doxorubicin. Doxorubicin treatment causes malfunctioning of the mitochondria by non-specific oxidative damage to the outer and the inner membranes, and by direct interaction with the mitochondrial DNA or enzymes involved in cell respiration.^{59,60} Doxorubicin delivery from **S3** in cells is expected to result in a decrease of cell viability. HeLa cells were treated with 20, 50, 150 and 200 $\mu\text{g/ml}$ of **S3** for 24 h and the cytotoxic effect of the released doxorubicin was evaluated by WST-1 assays. As it can be observed in Figure 8C a concentration-dependent decrease in living cells was found when compared to the untreated cells (100% viability). As an example when cells were treated with **S3** at a concentration of 150 $\mu\text{g/ml}$, around 60% of cells were effectively killed. Furthermore, the cytotoxic effect of **S3** was also clearly noted through changes in cell morphology and cells detachment, when compared with the untreated cells (control, see Figure 8A). CLSM images of HeLa cells incubated with **S3** at a concentration of 75 $\mu\text{g/mL}$ for 24h showed a dotted fluorescent patten, suggesting the internalization of nanoparticles and the GSH-triggered release of doxorubicin (see Figure 8B).

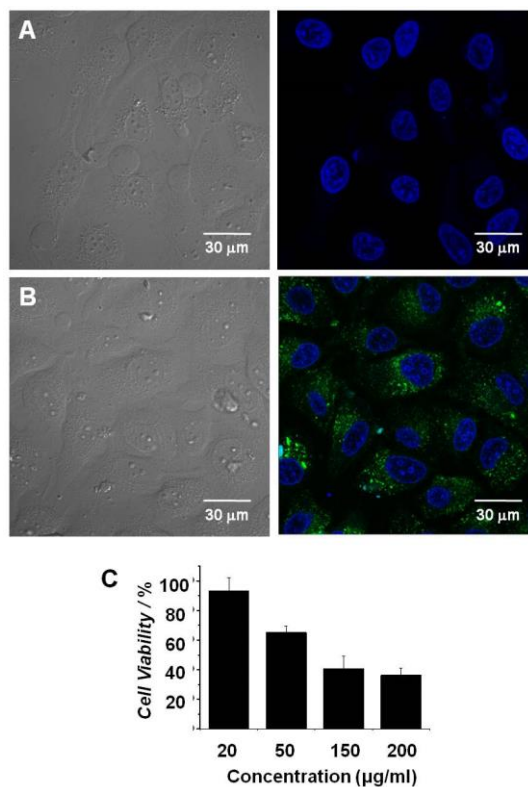


Figure 8. Cellular internalization and cell viability of **S3** gated-nanoparticles. a) Confocal microscopy images corresponding to untreated HeLa cells as a control of autofluorescence, b) HeLa cells treated with solid **S3** at 75 µg/mL concentration for 24h. Cellular uptake of the nanoparticles was evidenced by doxorubicin associated fluorescence (green) in the presence of DNA marker Hoechst 33342 (blue). c) WST-1 cell viability assay. HeLa cells were incubated for 24 h with **S3** at the indicated concentrations. Three independent experiments were performed and the data are represented as (mean ± SE).

CONCLUSIONS

In summary, we have described herein a new GSH-responsive, simple-to-prepare delivery system based in PEG-capped MSN. More specifically, hybrid materials with the dye safranin O or the anticancer agent doxorubicin as payloads and functionalized with PEG chains of different sizes in the pore entrances, were prepared. The preservation of the mesostructure in the final materials **S1**, **S2** and **S3** and the presence of capped pores were fully confirmed using typical

characterization techniques. The performance of the gated systems was assessed by kinetics release studies. The anchored PEG chains formed a dense barrier that inhibits the release of the cargo effectively. In contrast, when GSH was present, the disulfide bonds were cleaved allowing the release of the entrapped cargo. Moreover, as this active group is located near to the silica surface, the loaded safranin O can escape rapidly from the pore voids upon reduction of the S-S bond, achieving 90% of the maximum release of the entrapped guest in less than 1 h for **S1**. Finally, the performance of solids **S1** and **S3** in a cellular context was tested. The uptake of the gated nanoparticles, their aperture in the intracellular reductive environment and their ability to deliver the cargo in a controlled manner was confirmed. The results reported herein confirms that the use of simple disulphide bonds combined with highly hydrophilic and bio-compatible PEG derivatives is an easy way to design capped MSN that remain closed in non-reductive environments (for instance in plasma) yet deliver the cargo in an efficient way in the presence of a high concentrations of GSH (for instance in intracellular media).

AUTHOR INFORMATION

Corresponding Author

*E-mail: elazgi@upvnet.upv.es

*E-mail: rmaez@qim.upv.es

Author Contributions

The manuscript was written through contributions of all authors. All authors have given approval to the final version of the manuscript.

ACKNOWLEDGMENT

The authors thank the Spanish Government (Project MAT2012-38429-C04-01), the Generalitat Valenciana (Project PROMETEOII/2014/047) and the Universitat Politècnica de València (Project SP20120795) for support. C.G. and C.T also thanks the Spanish Ministry of Education for their FPU grants. They author also thank UPV electron microscopy and CIPF confocal microscopy services for technical support.

ASSOCIATED CONTENT

Supporting Information

Details of the chemicals, general techniques and characterization of all materials. This material is available free of charge via the Internet at <http://pubs.acs.org/>”).

REFERENCES

- [1] Allen, T. M.; Cullis, P. R. Liposomal drug delivery systems: from concept to clinical applications. *Adv. Drug Deliv. Rev.* **2013**, *65*, 36-38.
- [2] Gu, F.; Zhang, L.; Teply, B. A.; Mann, N.; Wang, A.; Radovic-Moreno, A. F.; Langer R.; Farokhzad, O. C. Precise engineering of targeted nanoparticles by using self-assembled biointegrated block copolymers. *Proc. Natl. Acad. Sci. USA* **2008**, *105*, 2586-2591.
- [3] Hadinoto, K.; Sundaresan, A.; Cheow, W. S. Lipid-polymer hybrid nanoparticles as a new generation therapeutic delivery platform: a review. *Eur. J. Pharm. Biopharm.* **2013**, *85*, 427-443.

- [4] Mattoussi, H.; Rotello, V. M. Inorganic nanoparticles in drug delivery. *Adv. Drug Deliv. Rev.* **2013**, *65*, 605-606.
- [5] Montenegro, J. M.; Grazu, V.; Sukhanova, A.; Agarwal, S.; de la Fuente, J. M.; Nabiev, I.; Greiner, A.; Parak, W. J. Controlled antibody/(bio-) conjugation of inorganic nanoparticles for targeted delivery. *Adv. Drug. Deliv. Rev.* **2013**, *65*, 677-688.
- [6] Padilla De Jesús, O. L.; Ihre, H. R.; Gagne, L.; Frechet, J. M.; Szoka, F. C. Jr. Polyester dendritic systems for drug delivery applications: in vitro and in vivo evaluation. *Bioconjug. Chem.* **2002**,*13*, 453-461.
- [7] Probst, C. E.; Zrazhevskiy, P.; Bagalkot, V.; Gao, X. Quantum dots as a platform for nanoparticle drug delivery vehicle design. *Adv. Drug Deliv. Rev.* **2013**, *65*, 703-718.
- [8] Torchilin, V. P. Recent advances with liposomes as pharmaceutical carriers. *Nat. Rev. Drug Discov.* **2005**, *4*, 145-160.
- [9] Zhang, L.; Chan, J. M.; Gu, F. X.; Rhee, J. W.; Wang, A. Z.; Radovic-Moreno, A. F.; Alexis, F.; Langer, R.; Farokhzad, O. C. Self-Assembled Lipid-Polymer Hybrid Nanoparticles: A Robust Drug Delivery Platform. *ACS Nano* **2008**, *2*, 1696-1702.
- [10] Mandal, B.; Bhattacharjee, H.; Mittal, N.; Sah, H.; Balabathula, P.; Thoma, L. A.; Wood, G. C. Core-shell-type lipid-polymer hybrid nanoparticles as a drug delivery platform. *Nanomedicine* **2013**, *9*, 474-491.
- [11] Greish, K. Enhanced permeability and retention (EPR) effect for anticancer nanomedicine drug targeting. *Methods Mol. Biol.* **2010**, *624*, 25-37.

- [12] Iyer, A. K.; Khaled, G.; Fang, J.; Maeda, H. Exploiting the enhanced permeability and retention effect for tumor targeting. *Drug Discov. Today* **2006**, *11*, 812-818.
- [13] Jain, R. K.; Stylianopoulos, T. Delivering nanomedicine to solid tumors. *Nat. Rev. Clin. Oncol.* **2010**, *7*, 653-664.
- [14] Maeda, H. The enhanced permeability and retention (EPR) effect in tumor vasculature: the key role of tumor-selective macromolecular drug targeting. *Adv. Enzyme Reg.* **2001**, *41*, 189-207.
- [15] Kresge, C. T.; Leonowicz, M. E.; Roth, W. J.; Vartuli, J. C.; Beck, J. S. Ordered mesoporous molecular sieves synthesized by a liquid-crystal template mechanism. *Nature*, **1992**, *359*, 710-712.
- [16] Zhang, Y.; Zhi, Z.; Jiang, T.; Zhang, J.; Wang, Z.; Wang, S. Spherical mesoporous silica nanoparticles for loading and release of the poorly water-soluble drug telmisartan. *J. Control. Release* **2010**, *145*, 257–263.
- [17] Rosenholm, J.M.; Mamaeva, V.; Sahlgren, C.; Lindén, M. Nanoparticles in targeted cancer therapy: Mesoporous silica nanoparticles entering preclinical development stage. *Nanomedicine (Lond)*, **2012**, *7*, 111-20
- [18] Coll, C.; Bernardos, A.; Martínez-Mañez, R.; Sancenón, F. Gates silica mesoporous supports for controlled release and signalling applications. *Acc. Chem. Res.*, **2013**, *46*, 339-349.

- [19] Fujiwara, M.; Terashima, S.; Endo, Y.; Shiokawa, K.; Ohue, H. Switching catalytic reaction conducted in pore void of mesoporous material by redox gate control. *Chem. Commun.* **2006**, 4635-4637.
- [20] Hernandez, R.; Tseng, H.-R.; Wong, J. W.; Stoddart, J. F.; Zink, J. I. An Operational Supramolecular Nanovalve. *J. Am. Chem. Soc.* **2004**, *126*, 3370-3371.
- [21] Gayam, S.R.; Wu, S.P. Redox responsive Pd(II) templated rotaxane nanovalve capped mesoporous silica nanoparticles: a folic acid mediated biocompatible cancer-targeted drug delivery system. *J. Mater. Chem. B*, **2014**, *2*, 7009-7016
- [22] Coll, C.; Casasús, R.; Aznar, E.; Marcos, M. D.; Martínez-Máñez, R.; Sancenón, F.; Soto, J.; Amorós, P. Nanoscopic hybrid systems with a polarity-controlled gate-like scaffolding for the colorimetric signalling of long-chain carboxylates. *Chem. Commun.* **2007**, 1957-1959.
- [23] Aznar, E.; Coll, C.; Marcos, M. D.; Martínez-Máñez, R.; Sancenón, F.; Soto, J.; Amorós, P.; Cano, J.; Ruiz, E. Borate-Driven Gate-like Scaffolding Using Mesoporous Materials Functionalised with Saccharides. *Chem. Eur. J.* **2009**, *15*, 6877-6888.
- [24] Climent, E.; Marcos, M. D.; Martínez-Máñez, R.; Sancenón, F.; Soto, J.; Rurack, K.; Amorós, P. The Determination of Methylmercury in Real Samples Using Organically Capped Mesoporous Inorganic Materials Capable of Signal Amplification. *Angew. Chem. Int. Ed.* **2009**, *48*, 8519-8522.
- [25] Aznar, E.; Villalonga, R.; Giménez, C.; Sancenón, F.; Marcos, M. D.; Martínez-Máñez, R.; Díez, P.; Pingarrón, J. M.; Amorós, P. Glucose-triggered release using enzyme-gated mesoporous silica nanoparticles. *Chem. Commun.* **2013**, *49*, 6391-6393.

- [26]Chen, X.; Cheng, X.; Soeriyadi, A. H.; Sagnella, S. M.; Lu, X.; Scott, J. A.; Lowe, S. B.; Kavallaris, M.; Gooding, J. J. Stimuli-responsive functionalized mesoporous silica nanoparticles for drug release in response to various biological stimuli. *Biomater. Sci.* **2014**, *2*, 121-130.
- [27]Yang, K. N.; Zhang, C. Q.; Wang, W.; Wang, P. C.; Zhou, J. P.; Liang, X. J. pH-responsive mesoporous silica nanoparticles employed in controlled drug delivery systems for cancer treatment. *Cancer Biol. Med.* **2014**, *11*, 34-43.
- [28] Xu, X.; Lü, S.; Gao, C.; Wang, X.; Bai, X.; Gao, N.; Liu, M. Facile preparation of pH-sensitive and self-fluorescent mesoporous silica nanoparticles modified with PAMAM dendrimers for label-free imaging and drug delivery. *Chem. Eng. J.* **2015**, *266*, 171-178
- [29] Yang, S.; Li, N.; Chen, D.; Qi, X.; Xu, Y.; Xu, Y.; Xu, Q.; Li, H.; Lu, J. Visible-light degradable polymer coated hollow mesoporous silica nanoparticles for controlled drug release and cell imaging. *J. Mater. Chem. B* **2013**, *1*, 4628-4636.
- [30]Mal, N. K.; Fujiwara, M.; Tanaka, Y. Photocontrolled reversible release of guest molecules from coumarin-modified mesoporous silica. *Nature*, **2003**, *421*, 350-353.
- [31] Aznar, E.; Marcos, M. D.; Martínez-Máñez, R.; Sancenón, F.; Soto, J.; Amorós, P.; Guillem, C. pH- and Photo-Switched Release of Guest Molecules from Mesoporous Silica Supports. *J. Am. Chem. Soc.* **2009**, *131*, 6833-6843.
- [32]De la Torre, C.; Agostini, A.; Mondragón, L.; Orzáez, M.; Sancenón, F.; Martínez-Máñez, R.; Marcos, M. D.; Amorós, P.; Pérez-Paya, E. Temperature-controlled release by changes

- in the secondary structure of peptides anchored onto mesoporous silica supports. *Chem. Commun.* **2014**, *50*, 3184-3186.
- [33] Dong, L.; Peng, H.; Wang, S.; Zhang, Z.; Li, J.; Ai, F.; Zhao, Q.; Luo, M.; Xiong, H.; Chen, L. Thermally and magnetically dual-responsive mesoporous silica nanospheres: Preparation, characterization, and properties for the controlled release of sophoridine. *J. Appl. Polym. Sci.* **2014**, *131*, 1-8
- [34] Ruiz-Hernández, E.; Baeza, A.; Vallet-Regí, M. Smart Drug Delivery through DNA/Magnetic Nanoparticle Gates. *ACS Nano* **2011**, *5*, 1259-1266.
- [35] Aznar, E.; Mondragón, L.; Ros-Lis, J. V.; Sancenón, F.; Marcos, M. D.; Martínez-Máñez, R.; Soto, J.; Pérez-Payá, E.; Amorós, P. Finely Tuned Temperature-Controlled Cargo Release Using Paraffin-Capped Mesoporous Silica Nanoparticles. *Angew. Chem. Int. Ed.* **2011**, *50*, 11172-11175.
- [36] Baeza, A.; Guisasola, E.; Ruiz-Hernández, E.; Vallet-Regí, M. Magnetically Triggered Multidrug Release by Hybrid Mesoporous Silica Nanoparticles. *Chem. Mater.* **2012**, *24*, 517-524.
- [37] Bringas, E.; Koysuren, O.; Quach, D. V.; Mahmoudi, M.; Aznar, E.; Roehling, J. D.; Marcos, M. D.; Martínez-Máñez, R.; Stroeve, P. Triggered release in lipid bilayer-capped mesoporous silica nanoparticles containing SPION using an alternating magnetic field. *Chem. Commun.* **2012**, *48*, 5647-5649.
- [38] Thomas, C. R.; Ferris, D. P.; Lee, J. H.; Choi, E.; Cho, M. H.; Kim, E. S.; Stoddart, J. F.; Shin, J. S.; Cheon, J.; Zink, J. I. Noninvasive remote-controlled release of drug molecules in

- vitro using magnetic actuation of mechanized nanoparticles. *J. Am. Chem. Soc.* **2010**, *132*, 10623-10625.
- [39] Mondragón, L.; Mas, N.; Ferragud, V.; de la Torre, C.; Agostini, A.; Martínez-Máñez, R.; Sancenón, F.; Amorós, P.; Pérez-Payá, E.; Orzáez, M. Enzyme-Responsive Intracellular-Controlled Release Using Silica Mesoporous Nanoparticles Capped with ϵ -Poly-L-lysine. *Chem. Eur. J.* **2014**, *20*, 5271-5281.
- [40] Patel, K.; Angelos, S.; Dichtel, W. R.; Coskun, A.; Yang, Y. W.; Zink, J. I.; Stoddart, J. F. Enzyme-Responsive Snap-Top Covered Silica Nanocontainers. *J. Am. Chem. Soc.* **2008**, *130*, 2382-2383.
- [41] Park, C.; Kim, H.; Kim, S.; Kim, C. Enzyme Responsive Nanocontainers with Cyclodextrin Gatekeepers and Synergistic Effects in Release of Guests. *J. Am. Chem. Soc.* **2009**, *131*, 16614-16615.
- [42] Bernardos, A.; Mondragón, L.; Aznar, E.; Marcos, M. D.; Martínez-Máñez, R.; Sancenón, F.; Soto, J.; Barat, J. M.; Pérez-Payá, E.; Guillem, C.; Amorós, P. Enzyme-Responsive Intracellular Controlled Release Using Nanometric Silica Mesoporous Supports Capped with “Saccharides”. *ACS Nano* **2010**, *4*, 6353-6368.
- [43] Agostini, A.; Mondragón, L.; Pascual, L.; Aznar, E.; Coll, C.; Martínez-Máñez, R.; Sancenón, F.; Soto, J.; Marcos, M. D.; Amorós, P.; Costero, A. M.; Parra, M.; Gil, S. Design of Enzyme-Mediated Controlled Release Systems Based on Silica Mesoporous Supports Capped with Ester-Glycol Groups. *Langmuir* **2012**, *28*, 14766-14776.

- [44] Climent, E.; Bernardos, A.; Martínez-Máñez, R.; Maquieira, A.; Marcos, M. D.; Pastor-Navarro, N.; Puchades, R.; Sancenón, F.; Soto, J.; Amorós, P. Controlled Delivery Systems Using Antibody-Capped Mesoporous Nanocontainers. *J. Am. Chem. Soc.* **2009**, *131*, 14075-14080.
- [45] Oroval, M.; Climent, E.; Coll, C.; Eritja, R.; Aviñó, A.; Marcos, M. D.; Sancenón, F.; Martínez-Máñez, R.; Amorós, P. An aptamer-gated silica mesoporous material for thrombin detection. *Chem. Commun.* **2013**, *49*, 5480-5482.
- [46] Climent, E.; Martínez-Máñez, R.; Sancenón, F.; Marcos, M. D.; Soto, J.; Maquieira, A.; Amorós, P. Controlled delivery using oligonucleotide-capped mesoporous silica nanoparticles. *Angew. Chem. Int. Ed.* **2010**, *49*, 7281-7283.
- [47] Giri, S.; Trewyn, B.G.; Stellmaker, M.P.; Lin, V.S.Y. Stimuli-Responsive Controlled-Release Delivery System Based on Mesoporous Silica Nanorods Capped with Magnetic Nanoparticles. *Angew. Chem. Int. Ed.* **2005**, *44*, 5038.
- [48] Koo, A. N.; Lee, H. J.; Kim, S. E.; Chang, J. H.; Park, C.; Kim, C.; Park, J. H.; Lee, S. C. Disulfide-cross-linked PEG-poly(amino acid)s copolymer micelles for glutathione-mediated intracellular drug delivery. *Chem. Commun.* **2008**, *48*, 6570-6572.
- [49] Mortera, R.; Vivero-Escoto, J.; II, Slowing.; Garrone, E.; Onida, B.; Lin, V. S. Cell-induced intracellular controlled release of membrane impermeable cysteine from a mesoporous silica nanoparticle-based drug delivery system. *Chem. Commun.* **2009**, *22*, 3219-3221.
- [50] Porta, F.; Lamers, G. E. M.; Zink, J. I.; Kros, A. Peptide modified mesoporous silica nanocontainers. *Phys. Chem. Chem. Phys.* **2011**, *13*, 9982-9985.

- [51] Thambi, T.; Deepagan, V. G.; Ko, H.; Lee, D. S.; Park, J. H. Bioreducible polymersomes for intracellular dual-drug delivery. *J. Mater. Chem.* **2012**, *22*, 22028-22036.
- [52] Wang, K.; Liu, Y.; Yi, W. J.; Li, C.; Li, Y. Y.; Zhuo, R. X.; Zhang, X. Z. Novel shell-cross-linked micelles with detachable PEG corona for glutathione-mediated intracellular drug delivery. *Soft Matter* **2013**, *9*, 692-699.
- [53] Wang, Y.C.; Wang, F.; Sun, T.M.; Wang, J. Redox-Responsive Nanoparticles from the Single Disulfide Bond-Bridged Block Copolymer as Drug Carriers for Overcoming Multidrug Resistance in Cancer Cells. *Bioconj. Chem.* **2011**, *22*, 1939-1945.
- [54] Hong, R.; Han, G.; Fernández, J. M.; Kim, B. J.; Forbes, N. S.; Rotello, V. M. Glutathione-Mediated Delivery and Release Using Monolayer Protected Nanoparticle Carriers. *J. Am. Chem. Soc.* **2006**, *128*, 1078-1079.
- [55] Jones, D. P.; Carlson, J. L.; Samiec, P. S.; Sternberg Jr, P.; Mody Jr., V. C.; Reed, R. L.; Brown, L. A. S. Glutathione measurement in human plasma. Evaluation of sample collection, storage and derivatization conditions for analysis of dansyl derivatives by HPLC. *Clin. Chim. Acta* **1998**, *275*, 175-184
- [56] Estrela, J. M.; Ortega, A.; Obrador, E. Glutathione in cancer biology and therapy. *Critical Rev. Clin. Lab. Sci.* **2006**, *43*, 143-181
- [57] Yeh, C. C.; Hou, M. F.; Wu, S. H.; Tsai, S. M.; Lin, S. K.; Hou, L. A.; Ma, H.; Tsai, L.Y. A study of glutathione status in the blood and tissues of patients with breast cancer. *Cell Biochem. Funct.* **2006**, *24*, 555-559.

[58] Brunauer, S.; Emmett, P. H.; Teller, E. Adsorption of Gases in Multimolecular Layers. *J. Am. Chem. Soc.* **1938**, *60*, 309-319.

[59] Finsterer, J.; Ohnsorge, P. Influence of mitochondrion-toxic agents on the cardiovascular system. *Regul Toxicol Pharmacol*, **2013**, *67*, 434-445.

[60] Yang, F.; Teves, S.S.; Kemp, C. J.; Henikoff, S. Doxorubicin, DNA torsion, and chromatin dynamics. *Biochim. Biophys. Acta* **2014**, *1845*, 84-89.

TOC Graphic

